An *AC* modulated Near InfraRed gain calibration system for a 'Violin-Mode' transimpedance amplifier, intended for advanced LIGO suspensions

N.A. Lockerbie and K.V. Tokmakov

SUPA (Scottish Universities Physics Alliance) Department of Physics, University of Strathclyde, 107 Rottenrow, Glasgow G4 0NG, UK.

Abstract. The background to this work was a prototype shadow sensor, which was designed for retro-fitting to an Advanced LIGO (Laser Interferometer Gravitational wave Observatory) test-mass/mirror suspension, in which a 40 kg test-mass/mirror is suspended by four approximately 600 mm long by 0.4 mm diameter fused-silica suspension fibres. The shadow sensor comprised a LED source of Near InfraRed (NIR) radiation, and a 'tall-thin' rectangular silicon photodiode detector, which together were to bracket the fibre under test. The photodiode was positioned so as to be sensitive (primarily) to transverse 'Violin-Mode' vibrations of such a fibre, via the oscillatory movement of the shadow cast by the fibre, as this moved across the face of the detector. In this prototype shadow sensing system the photodiode was interfaced to a purpose-built transimpedance amplifier, this having both *AC* and *DC* outputs. A quasi-static calibration was made of the sensor's *DC* responsivity, i.e., incremental rate of change of output voltage versus fibre position, by slowly scanning a fused-silica fibre sample transversely through the illuminating beam. The work reported here concerns the determination of the sensor's more important *AC* (Violin-Mode) responsivity. Recognition of the correspondence between direct *AC* modulation of the source, and actual Violin-Mode signals, and of the transformative rôle of the *AC*/*DC* gain ratio for the amplifier, at any modulation frequency, *f*, resulted in the construction of the *AC*/*DC* calibration source described here. A method for determining in practice the transimpedance *AC*/*DC* gain ratio of the photodiode and amplifier, using this source, is illustrated by a specific numerical example, and the gain ratio for the prototype sensing system is reported over the frequency range 1 Hz–300 kHz.

PACS numbers: 04.80.Nn, 84.30.-r, 06.30.Bp, 07.07.Df, 07.57.-c

1. Introduction

A prototype system of four shadow-sensors was designed to be retro-fitted to an advanced LIGO (Laser Interferometer Gravitational wave Observatory) test-mass/mirror suspension, in which a 40 kg test-mass is suspended by four fused silica fibres, the dimensions of the fibres being approximately 600 mm long by 0.4 mm in diameter [1–6]. Initially, the shadow-sensor—one intended for each suspension fibre—consisted of a single 'tall, narrow' rectangular silicon photodiode (*Hamamatsu* S2551, [7]), together with a collimated source of Near InfraRed (NIR: λ = 880–890 nm) illumination—this casting a shadow of the illuminated fibre over one vertical edge the facing detector. In later work, however, a higher displacement sensitivity (but more elaborate) 'synthesized split-photodiode' detector was employed [8,9]. The principal purpose of the full detection system, using either detector, was to monitor any lateral 'Violin-Mode' resonances that might be excited in these fibres, as well as to check for any 'large' amplitude, low frequency, 'pendulum-mode' motion of the test-mass and its suspension fibres (at ~ 0.6 Hz), such that all of this oscillatory motion then could be cold-damped, actively [10]. Consequently, the purpose-built Violin-Mode (*VM*) amplifier, which was interfaced to the detector, had two separate outputs: a relatively low (transimpedance) gain '*DC*' output, to cater for large pendulum-mode excursions of the monitored fibre (up to at least 0.14 mm, peak-peak), and a much higher transimpedance gain, but lower displacement-sensing range, *AC* output, this being intended for detecting *VM* oscillations—ultimately, down to below 100 picometres (rms), in 1 second, at frequencies in the range 500 Hz–5 kHz [8,9,11]. Sensing *VM* oscillations was

the primary function of the shadow-sensor, and an important ancillary rôle of the amplifier's separate *DC* and *AC* outputs was to allow an actual calibration of the *VM* (*AC*) displacement responsivity of the detection system to be made. This calibration was accomplished in two stages.

Firstly, a 0.4 mm diameter silica-fibre sample was translated at a steady rate (~50 μm s^{-1}) transversely through the shadow-sensor's illuminating NIR beam, and the resulting 'notch' was recorded in the amplifier's *DC* output voltage as a function of fibre position—the notch occurring as the fibre's shadow passed across the face of the photodiode detector. The shadow-notch voltage then was differentiated off-line, as a function of fibre position, so as to yield the rate-of-change of detected *DC* voltage with incremental fibre displacement, versus mean fibre position. This quantity was the *DC* (quasi-static) responsivity of the sensor to fibre displacement. It was measured in kilovolt(s) per metre (typically), reaching its maximum value when the fibre's shadow overlapped—and its centre was aligned with—just one vertical edge of the photodiode detector. This stage of the calibration process has been reported elsewhere, in connection with the split-photodiode detector [12]. Following such a calibration procedure, any additional low-level oscillation of the shadow, at a given *VM* frequency, and with a fixed peak-peak amplitude, would sweep the shadow back-and-forth across the face of the photodiode detector—between effectively two fixed (fibre) positions; and, as a result of the calibration, the *DC* (quasi-static) responsivity would have been established over this span. Unfortunately, the response of the attendant amplifier to *AC* photocurrents was different from its response to the (change in) *DC* photocurrent, over the same excursion of fibre position; but if the ratio of the amplifier's *AC* to *DC* responses could be found, then the detection system's *AC* responsivity to shadow displacement could be inferred from its measured *DC* responsivity.

Moreover, it was appreciated that a modulation of the photodiode's irradiance arising from an oscillating shadow (at a given *VM* frequency), could not be distinguished from that due to an intrinsic modulation at source of the incident beam's intensity, at the same frequency. Thus, if the ratio of the detector's relative transimpedance sensitivity to *AC* photocurrents (at 500 Hz, say), to its *DC* sensitivity, were known, then a calibration of the photodiode detector plus amplifier at *DC* would allow the *AC* responsivity at that frequency to be deduced—the photodiode used responded equally well to *AC* and *DC* excitation at such low frequencies. However, in order to accomplish this, a method needed to be found for illuminating the photodiode detector with a NIR beam having both a steady level of mean irradiance, and an accurately known (relative) depth of sinusoidally modulated irradiance—at a controlled frequency. The mean level of irradiance would generate the amplifier's *DC* output signal, whilst the sinusoidal modulation would generate the corresponding '*VM*' (*AC*) output, so that the ratio of these signals—and so their relative responsivities—could be linked. This was the second stage of the calibration process, and the approach that was taken, together with the results obtained, are reported below. It turned out that the *VM* (*AC*) displacement responsivity would be found to lie in (typically) the megavolt(s) per metre of fibre displacement range.

2. The prototype Violin-Mode amplifier

2.1. Separating the photocurrents: the amplifier's DC and AC outputs

The circuit diagram of the prototype Violin-Mode amplifier is shown in Figure 1, a subsequent dual-input version being covered in [10, and references therein]. Here, a *Hamamatsu* S2551 photodiode has a small reverse bias (~0.5 V) due the self-biasing action of the JFET (BF862) transistor, at a drain current ~1.1 mA. The source-follower action of the JFET transistor prevented *AC* voltages from being impressed across the photodiode, and

its connecting cable, thereby reducing considerably any 'noise-gain peaking' in the amplifier's *AC* response [10]. In the Figure, the photodiode detector is shown being illuminated from the left by a NIR beam of constant mean intensity, this beam having an additional small-amplitude sinusoidal modulation of its intensity, at a known frequency. Thus, if the reverse photocurrent generated in the photodiode by the beam is I_{photo}, as indicated, then $I_{photo} = I_{DC} + i$, where I_{DC} is a steady *DC* photocurrent, and i is an incremental *AC* photocurrent, due to the modulation, superimposed onto the steady *DC* current flow.

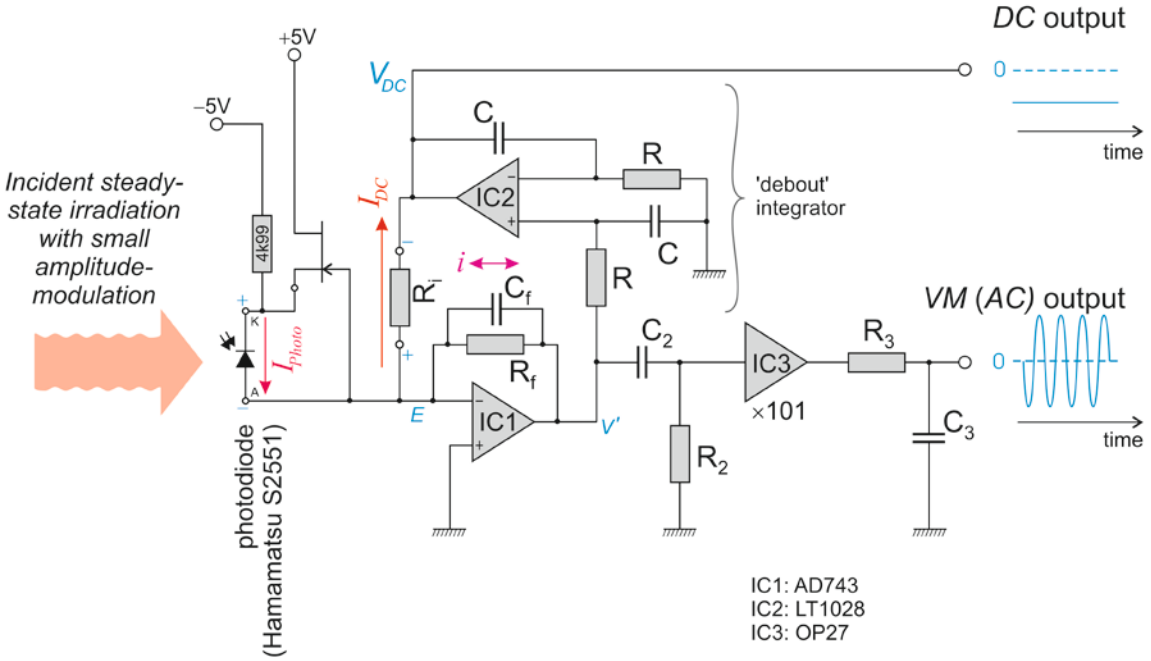

Figure 1. Circuit diagram of the prototype *VM* amplifier (±15 V supply omitted). In the Figure, Near InfraRed radiation, incident on the photodiode from the left, consists of a steady flux with a small superimposed intensity modulation. The illumination of the reverse-biased photodiode causes a photocurrent I_{photo} to flow through it, as indicated, where $I_{photo} = I_{DC} + i$. Here, I_{DC} is a steady *DC* photocurrent, and i is the incremental *AC* photocurrent due to the modulation. The 'debout' (French for 'upright,' or non-inverting) integrator in the circuit, taking as its input the voltage *V'*, forces these two photocurrents to follow the different transduction paths indicated in the Figure. This action is explained in the text. Separately, the JFET transistor in the circuit mitigates any 'noise-gain peaking' due to the capacitance of the photodiode (please refer to the text). In the Figure: R = 100k, C = 100n, R_i = 120k, R_f = 1M2, C_f = 10p7, C_2 = 100n, R_2 = 10k, R_3 = 3k, and C_3 = 1000p.

In Figure 1, IC1 and IC2 are op-amps, and IC3 is a simple non-inverting (op-amp based) amplifier, with an *AC* voltage gain of ×101. The point labelled with the voltage *V'* in the Figure is the input to a 'debout' integrator, this being constructed around IC2, along with the two resistors R and capacitors C. The point labelled *E* in the circuit is a virtual-Earth point, due to the negative feedback around IC1. Negative feedback around IC2 (the integrator), on the other hand, forces its mean steady-state input voltage ($V'|_{mean}$) always to be very close to zero volts. Were $V'|_{mean}$ to be non-zero, the integrator's output voltage would drift over time; but with zero average input to the integrator, the integrator's output must be frozen at whatever voltage happened to be historically its most recent value. Consequently, there can be no *mean* voltage difference between points *E* and *V'* in the circuit. Therefore, no *DC* current can flow through feedback resistor, R_f. Accordingly, all of the photocurrent I_{DC} must flow out of the photodiode's anode, at point *E*, down through resistor R_i, as shown, and into the output (acting as a current sink) of IC2. Consequently, the voltage marked V_{DC} in the Figure is an analogue of this *DC* photocurrent, such that the *DC* output voltage of the

amplifier as a whole can be written $V_{DC} = -I_{DC}\,R_i$. It is always a negative voltage. Ignoring the sign, R_i (= 120 kΩ) is seen to be the *DC* transimpedance gain of the amplifier.

The output voltage of the sluggish integrator (output of IC2) governs the voltage drop across resistor R_i; but the integrator's output is unable to change rapidly, and so relatively high frequency voltage signals cannot be impressed across resistor R_i, by IC2. In consequence, and unlike the *DC* photocurrent, the photodiode's modulation-induced *AC* photocurrent, *i*, cannot flow through resistor R_i. Instead, it must flow through the parallel combination of R_f–C_f, i.e., through the feedback path around IC1—whose output voltage can change quickly, if necessary. Consequently, the *DC* and *AC* photocurrents are forced to follow different amplification paths, as indicated in Figure 1. At normal *VM* signal frequencies the *AC* photocurrent actually flows through resistor R_f, alone, such that a (zero-mean) *AC* signal is present at the output of IC1, with $V'|_{AC} = -i\,R_f$. Here, a positive value of the incremental *AC* photocurrent *i* is taken to flow in the same sense as the *DC* photocurrent, I_{DC}. Therefore, $-R_f$ is seen to be the *AC* transimpedance gain of the amplifier, if taken just to the output of IC1. However, this output voltage is high-pass filtered by C_2–R_2, before being post-amplified by IC3, which is an *AC* amplifier, having a non-inverting voltage gain of ×101. The output of IC3 is then low-pass filtered by R_3–C_3, so as to roll-off the *AC* signal gain more strongly above frequencies ~12 kHz, where there are no *VM* signals of interest. Thus, the *AC* transimpedance gain of the amplifier is seen to be effectively $-101R_f$, mid-band (i.e., at 1.71 kHz), or 121.2 MΩ—once again, ignoring the sign.

In summary, the *DC* transimpedance gain of this amplifier is (–)120 kΩ, whilst the corresponding *AC* transimpedance gain is (nominally) (–)121.2 MΩ—mid-band. Therefore, the ratio of its *AC* to *DC* responses *to the same change in photocurrent* was set at nominally 1010, mid-band. In fact, the bandwidth of the prototype amplifier was circumscribed deliberately by 4 poles and 2 zeroes in its frequency response, such that its *AC* passband extended from below the fundamental *VM* frequency (500 Hz) up to at least the tenth of its harmonics, i.e. up to >5 kHz. This fairly narrow bandwidth resulted in the passband's plateau peaking, theoretically, at the slightly lower mid-band value of 1004.

2.2. The prototype VM amplifier's output frequency responses

The prototype *VM* amplifier, whose circuit is shown in Figure 1, can be analysed straightforwardly to yield, in terms of the complex frequency s, a transimpedance relationship at its *DC* output of the form

$$\frac{V_{DC}}{I_{DC}} = -\frac{R_f}{\left(s^2 CRC_f R_f + sCR + R_f/R_i\right)} \qquad (1).$$

Clearly, for a strictly *DC* component of photocurrent (i.e., s = 0) Equation 1 reduces to the simple expression $V_{DC} = -I_{DC}R_i$, as mentioned in §2.1. For the component values used (given in the caption of Figure 1), the expression in equation 1 is effectively that of a low-pass response, with a dominant pole at 161 Hz (and a second, HF, pole at 12.2 kHz). Therefore, 0.6 Hz pendulum-mode signals would be passed without attenuation, at this *DC* amplifier output. In a similar fashion, the *ratio* of the amplifier's *AC* response to a *VM* signal photocurrent, to its *DC* response to a steady quiescent photocurrent, i.e., the amplifier's ratio of transimpedance gains, can be found to be

$$\frac{V_{AC}}{V_{DC}(s=0)} = \frac{A(R_f/R_i)s^2 CRC_2R_2}{\left(s^2 CRC_f R_f + sCR + R_f/R_i\right)(sC_2R_2+1)(sC_3R_3+1)} \qquad (2).$$

Equation 2 evidently possesses two zeroes (at s = 0), and four poles, so as to delimit a passband—centred around the *VM* frequencies of interest—as mentioned in §2.1. The magnitude of Equation 2 is plotted as the dashed line in Figure 5 as a function of the frequency f (in Hz), with A = 101, and using the component values given in the Figure 1 caption. Here, the value of the small capacitor C_f ('10 pF') was used as a fitting parameter.

2.3. Practical Near InfraRed (NIR) gain calibration

Equation 2 expresses the relative sensitivity of the amplifier's *AC* and *DC* outputs to changes in photocurrent due to *the same* displacement of a fibre's shadow falling across (the edge of) the photodiode detector: in the one case a change occurring at a frequency s (= jω, for a sinusoidal modulation at angular frequency ω, where $j = \sqrt{-1}$, and $\omega = 2\pi f$); and in the other a change occurring from one steady value to another. It is this expression of relative dependency which motivated the practical calibration of the *VM* (*AC*) displacement responsivity, at a given modulation frequency, *f*.

A calibration system was designed and built in order to measure the ratio of the *AC* to *DC* responses of an S2551 photodiode, connected to the prototype amplifier. A short (< 80 mm) miniature coaxial lead was used to make this electrical connection, but, in order to simulate the capacitance of a coaxial cable 6+ m long (as might be used in a Gravitational Wave Detector environment), a 680 pF capacitor was placed in parallel with the photodiode.

3. A calibration system for both *AC* and *DC* responsivities

3.1. The calibration source

The calibration system needed to irradiate the amplifier's single photodiode detector with a

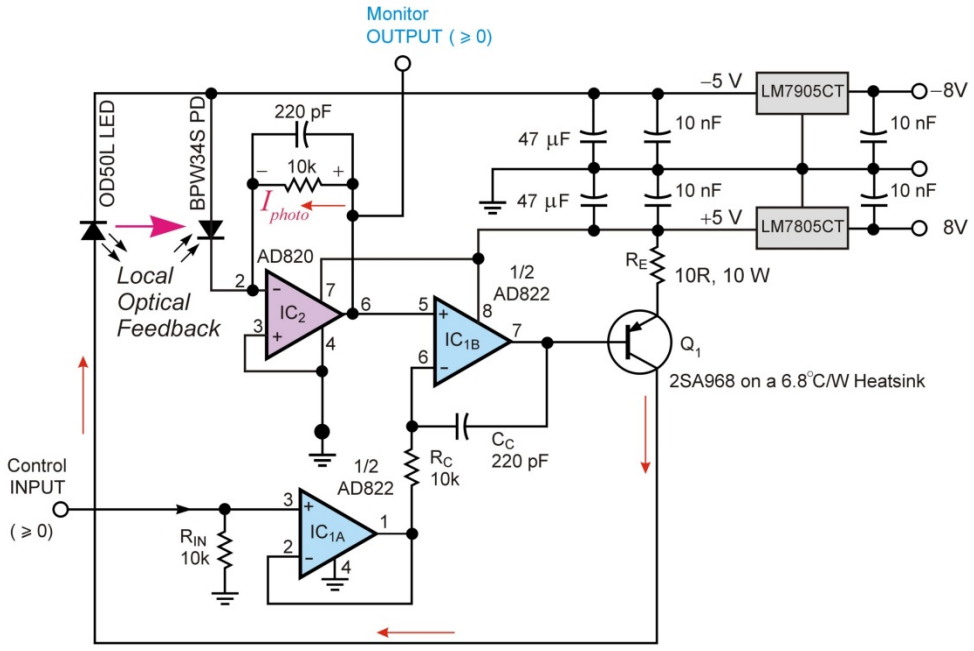

Figure 2. InfraRed modulation circuit derived from an original article by Lukasz Sliwczynskia and Marcin Lipinski [13]. Two voltage regulators supply the ±5 V rails for the Near InfraRed intensity controlling and modulation circuit. Via local, optical, feedback, the NIR beam emitted by the OD50L LED was a precise analogue in its intensity of the voltage at the 'Control INPUT'—for both the *DC* level and for any *AC* modulation superimposed on top of this level, i.e., for the sum of any such voltages, provided the sum was ≥ 0.

very low intensity beam from a NIR LED, the beam consisting of a steady component of fixed intensity, plus a small sinusoidal intensity-modulation on top of this, at a known

frequency, *f*. Figure 2 shows the circuit diagram of the calibration source for the photodiode/amplifier that was used in this work. The NIR beam's modulation-controlling circuit was based on a published article which described the control of an IPL10530KAL device [13]. In a single package this device contained a LED emitter, and an intensity-monitoring photodiode, as well as a transimpedance amplifier. In this work, however, separate devices were used: a discrete BPW34S photodiode (PD) was mounted off-axis at a distance of approximately 15 mm from the lens of a high-power OD50L, NIR LED, emitter (λ = 880 nm), the PD being located at an angle of approximately 5° from the LED's beam-axis. The PD monitored the emitter's output beam intensity, whilst an AD820 op-amp, together with its indicated feedback components, acted in the transimpedance rôle.

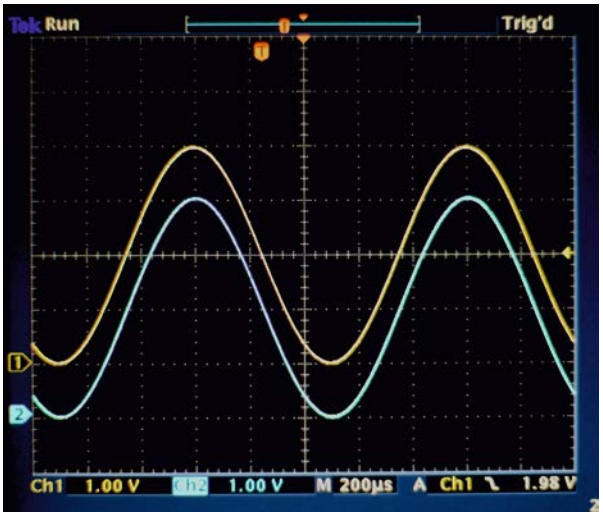

Figure 3. Example of the optical feedback control of emitted intensity. In this example a very high level of relative modulation was used. Upper trace (yellow): Control INPUT to the circuit of Figure 2, showing a 'command' voltage in the form of a 1 kHz, 4.0 volt peak-peak, modulation, about a steady 2.0 volt *DC* level. Lower trace (blue): Monitor OUTPUT (offset down the screen by approximately 1 volt). Here, local, optical, negative feedback between the OD50L LED and the local BPW34S silicon photodiode has forced the intensity of the beam emitted by the NIR LED to be a close analogue of the command voltage—even under these rather extreme conditions (+5 volt supply to the circuit, and total input control voltage descending to zero volts).

The Control INPUT voltage to the circuit shown in Figure 2 consisted of a positive *DC* level, about which a (generally) small amplitude sinusoidal *AC* modulation was added, this modulation being at a fixed frequency, *f*, in the range 1 Hz– 300 kHz. A *DC* current of typically ~ 200 mA was generated by the voltage applied to this Control input. It was sourced by the pnp transistor, Q_1, which powered the OD50L emitter. Local, optical, feedback via the BPW34S photodiode then slaved the LED's emitted output intensity to be a very precise analogue of the control input voltage (both *DC* level and *AC* modulation)—and this could be verified at the circuit's Monitor output, where, under correct operation, Monitor OUTPUT voltage = Control INPUT voltage. Figure 3 shows an example of this action. In this way, and via the linearity of the off-axis photodiode and its transimpedance amplifier, the intensity of the NIR beam emitted by the LED became a very close analogue of the Controlling input signal—for both the *DC* level and the *AC* modulation.

3.2. AC and DC relative gain measurements

Figure 4 shows schematically a modulated NIR beam, coming from the OD50L LED, being used to illuminate the prototype amplifier's photodiode, via a pinhole in a mask. The LED was positioned with the front of its lens approximately 35 mm from the mask, and with its beam incident normally onto the mask. The pinhole was 0.35 mm in diameter. On the Control INPUT side of the source, as shown in Figure 2, both the *DC* and modulation

(peak-peak) levels were noted for the particular modulation frequency being used. These waveforms then were checked for fidelity (i.e., proper feedback control) at the Monitor OUTPUT of the source. The resulting *AC* and *DC* output signals from the prototype amplifier also were measured at this time. The ratio of the amplifier's *AC*/*DC* gain then was computed from these four measured signals, for that particular modulation frequency—as described in the following example (illustrated in Figure 4).

The three graphs shown in Figure 4 are actual oscilloscope screen shots taken during a measurement: at the lower right of the Figure the Control input is seen to consist of a *DC* level = 2.151 V, plus a small sinusoidal modulation [58.0 mV (peak-peak), at 1 kHz]. Here, the Monitor output signal was indistinguishable from that at the Control input—over the frequency range 1 Hz ≤ f ≤ 300 kHz; in the lower left screen shot the amplifier's *DC* output = –1.023 V; and in the top screen shot the amplifier's *AC* output = 27.33 V (peak-peak)—in anti-phase with the input modulation at 1 kHz, as expected. Therefore, in this example the measured *AC/DC* gain ratio = (27.33/58.0e–3) / (1.023/2.151) = 991 (± 4), at 1 kHz.

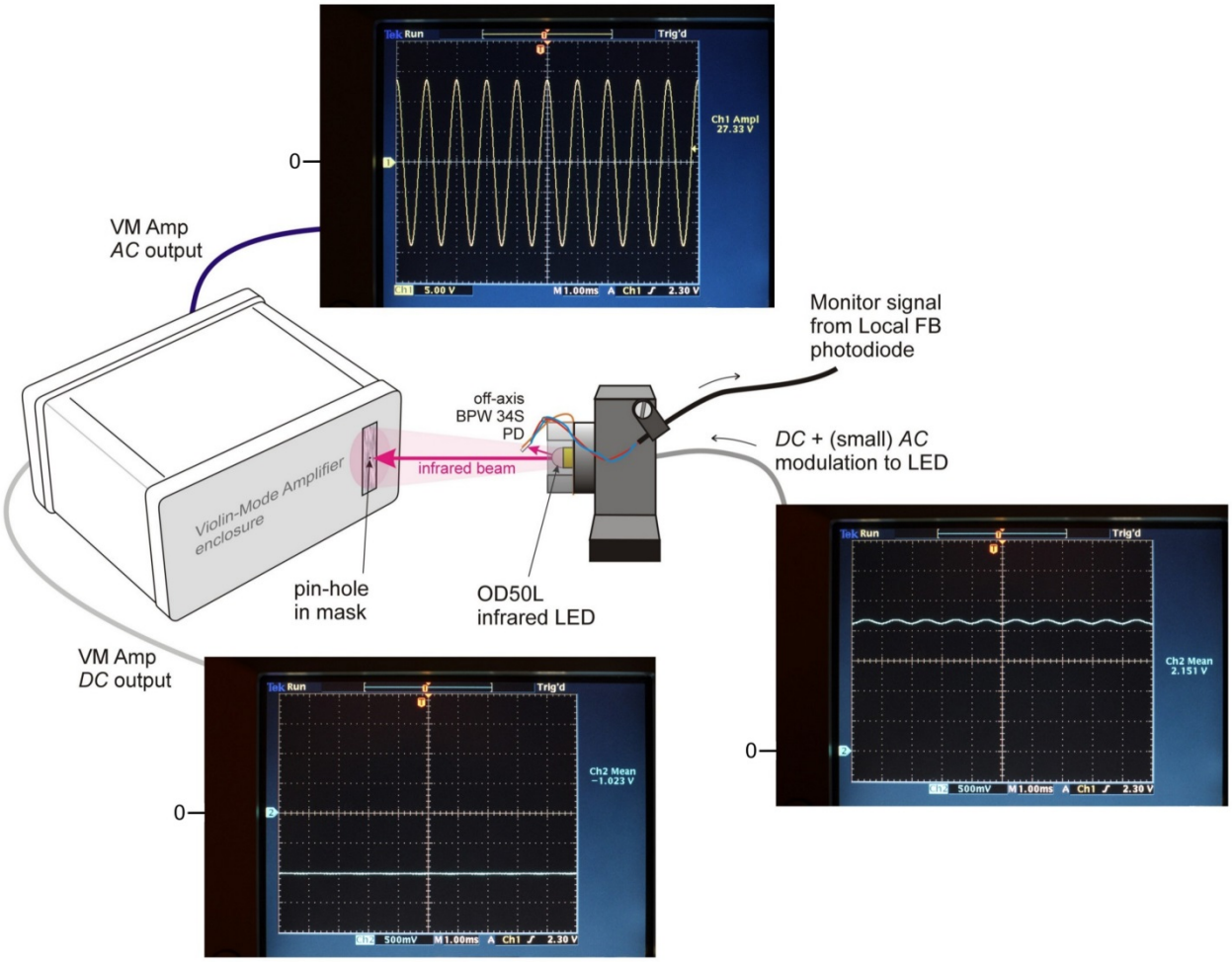

Figure 4. Schematic diagram showing a measurement of the *AC*/*DC* gain ratio of the photodiode/prototype amplifier at a particular frequency, *f* (here, *f* = 1 kHz). The infrared beam from the OD50L infrared LED was incident onto the amplifier's S2551 photodiode via a pin-hole in an aluminium foil mask. The three graphs are actual oscilloscope screen shots: on the right the Control Input = 2.151 V + (58.0 $mV_{p\text{-}p}$, 1 kHz, modulation); in the lower left screen shot the amplifier's *DC* output = –1.023 V; and in the top screen shot the amplifier's *AC* output = 27.33 $V_{p\text{-}p}$, this being in anti-phase with the input modulation at 1 kHz, as expected. The *DC* zero voltage levels have been emphasized in each of the screen shots. Please refer to the text for the *AC/DC* gain ratio calculation.

This procedure was repeated for modulation frequencies in the range 1 Hz–300 kHz, although, towards the lower end of this frequency range, the amplitude of modulation had to be increased—so that the *AC* response might become more easily measurable.

The results of such measurements as a function of the modulation frequency *f* are shown in Figure 5. Clearly, the measurements followed the theoretical expectation very well up to ~ 100 kHz, i.e., well above the required *VM* bandwidth, which extended from 500 Hz–5 kHz. Indeed, Equation 2 gives the theoretical *AC*/*DC* gain ratio to be 927.1 at 500 Hz, and 994.2 at 1 kHz, whereas the measured values, using the method shown in Figure 4, gave this same ratio as being 922.5 ± 4 at 500 Hz, and 991 ± 4 at 1 kHz.

For the numerical example illustrated in Figure 4, the *AC* responsivity = 991 × the *DC* responsivity (measured separately, as explained in §1; and in [12]), at 1 kHz.

In fact, a maximum *DC* responsivity of 1.26 $kV.m^{-1}$ was measured using the prototype sensor discussed here. Therefore, the measured *AC*/*DC* transimpedance gain ratio of 922.5 for this sensor, at 500 Hz, translated into a maximum *VM* (*AC*) responsivity of 1.16 MVm^{-1}, at that frequency.

3.3. The AC/DC ratio of transimpedance gains, measured as a function of frequency

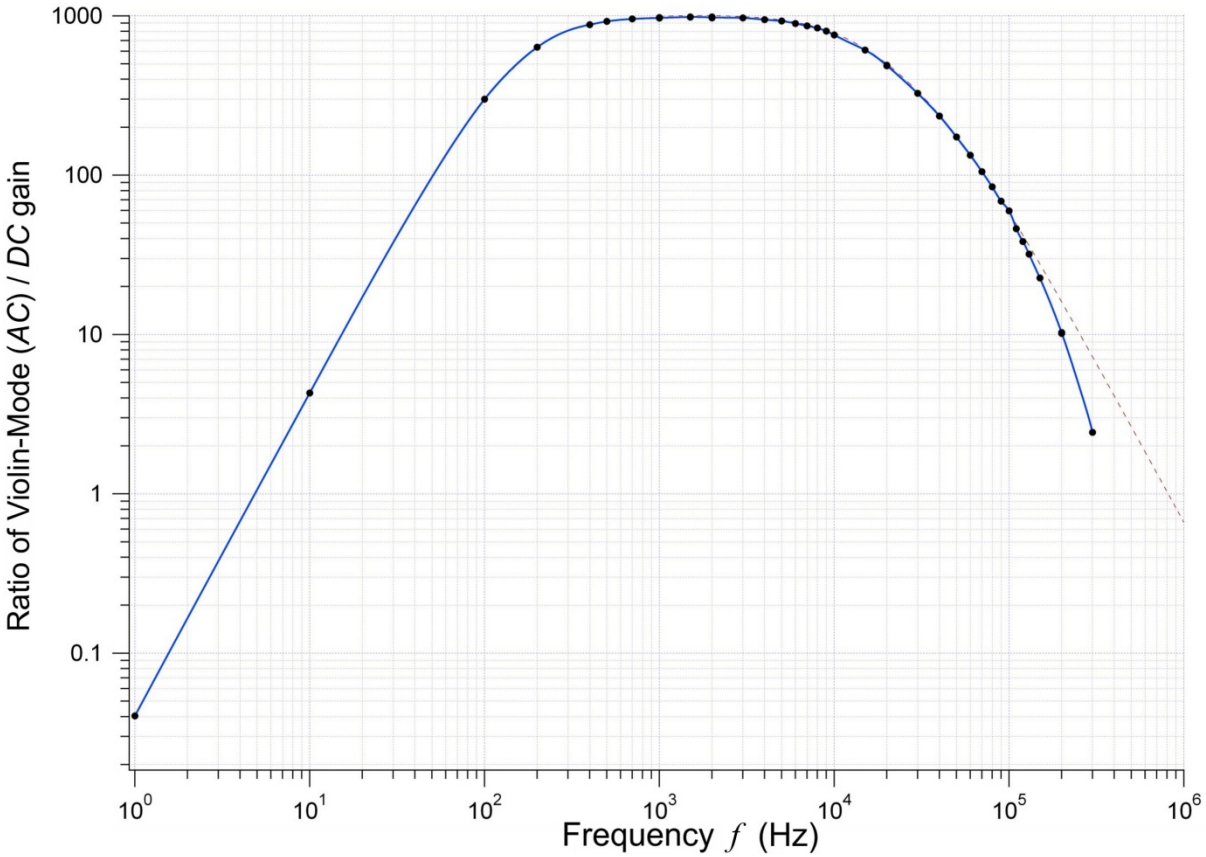

Figure 5. Measured ratio of the *AC*/*DC* (s = 0) transimpedance gains for the prototype amplifier/photodiode, as a function of the modulation frequency, *f*, using the calibration apparatus shown in Figures 2 and 4. The solid data points are measurements made using the technique shown in Figure 4, the (blue) full-line through these data being simply a guide to the eye. The dashed line running from 1 Hz–1 MHz (largely obscured) is the magnitude of the theoretical gain ratio, given by Equation 2. For these measurements an additional 680 pF capacitor was placed in parallel with the single Hamamatsu S2551 photodiode, in order to simulate the capacitance of 6+ m of co-axial cable running between the photodiode and the amplifier (please refer to the text). The -3 dB frequencies for the ratio of the *AC*/*DC* gains were found here to be 241 Hz, and 12074 Hz.

The measured ratio of the *AC/DC* (s = 0) transimpedance gains for the prototype amplifier/ photodiode shadow detector, shown in Figure 5, clearly followed the theoretical curve (indicated by the dashed line in the Figure) very well indeed, up to ~100 kHz. Evidently, the amplifier was functioning as anticipated, from the theory given in §1 and §2. One small feature of the measurements of the *AC*/*DC* gain ratio that was noticed, however, was that between its two −3 dB points (give in the caption to Figure 5), where this ratio approached a value of 1000, the measured values tended to lie slightly below (< 1% below) the theoretical expectations. It could be argued that only 1% tolerance resistors had been used in constructing the amplifier, and so the agreement was unexpectedly close, anyway; but then this shortfall did not extend to either lower, or higher frequencies, f (for f < 100 kHz, that is). An alternative explanation might be that in this frequency regime the *AC* output signals were typically ~27 volts (peak-peak). No obvious distortion was seen in such cases, but this level of excursion lies close to the maximum voltage swing of an OP27E op-amp's output—with a ±15 V supply. In retrospect, it might have been better to have limited such voltage swings to ~25 volts (peak-peak), say. The fall-off in the *AC*/*DC* gain ratio above ~100 kHz, however, was due to the effective bandwidth of the *AC* amplifier built around IC3, which was expected to be only ~80 kHz. This additional roll-off in response towards higher frequencies was seen as being positively beneficial, however—from the point of view of reducing noise.

4. Conclusions

A bench measurement of the shadow-sensor's quasi-static responsivity to suspension fibre displacement (or *DC* responsivity), clearly allows the more valuable *AC* responsivity to be inferred—with a high degree of confidence, from the agreement with theory—at any given *VM* frequency; but the use of a transimpedance amplifier having two separate outputs (*DC* and *AC*) is then a *sine qua non*. Moreover, the ratio of *AC/DC* transimpedance gains for the amplifier then has to be found, as shown in Figure 5, and, in order to make that measurement, the modulated illuminating source, as described here in §3.1 and §3.2, has turned out to be indispensable. In contrast, trying to vibrate the entire fibre, bodily, within the illuminating beam, as an isolated entity (having no physical supports), and with an accurately-known amplitude of 1.00 μm, say, across the whole frequency range, was never an option.

The single photodiode detector / prototype transimpedance amplifier discussed here was developed, eventually, into the split-photodiode / dual-input transimpedance amplifier, discussed in [9,11]; and, for comparison, the *DC* responsivity of this later development was measured at 10.7 kVm^{-1}, averaged over its four sensors, compared with the 1.26 $kV.m^{-1}$ reported here. The effective *AC/DC* gain ratio for the dual-input amplifier was 904 ± 4 at 500 Hz—determined by placing the pinhole mask over each detector element, separately—leading to a high (average) *VM* responsivity of 9.65 MVm^{-1}, at this frequency.

At the time of writing neither the Violin-Mode amplifier and sensor system described here, nor its successor [8,9,11,14], has been adopted for aLIGO, and, indeed, the need for separate *VM* sensing and damping has not yet been demonstrated. The current baseline solution is to use aLIGO's Arm Length Stabilization system as a *VM* sensor / damper [15]. In fact, the issue of vacuum compatibility remains unresolved for the *VM* sensor described here, and its successor, because the *Hamamatsu* photodiodes used for the detector elements had been encapsulated, using an unknown epoxy. However, were it to become necessary, the issue of the epoxy for the photodiodes from this, or another, manufacturer probably could be resolved, and the LEDs and other components used are likely to prove vacuum compliant, or have vacuum-compliant alternatives.

5. Acknowledgements

We thank the IGR, University of Glasgow, Scotland, UK, particularly Ken Strain and Angus Bell, for their encouragement with this work. Thanks go to Norna Robertson and Calum Torrie of Caltech and the IGR, Alberto Vecchio of the University of Birmingham, and Justin Greenhalgh of the CCLRC (RAL), for their oversight of, and assistance with, this work. We are grateful to the staff of the Physics Department's Electronics Workshop, and the Science Faculty's Mechanical Workshop, at the University of Strathclyde, for their careful construction of most of the component parts used in this work, and we would also like to thank the company *Bar Knight Precision Engineers Ltd.* of Clydebank, Scotland, for their very good, and timely, machining work. Finally, we are grateful for the support of grant STFC PP/F00110X/1, which sustained this work.

References

[1] Harry G M (for the LIGO Scientific Collaboration) 2010 Advanced LIGO: the next generation of gravitational wave detectors. *Class. Quantum Grav.* **27** 084006 (12pp).

[2] Raab F J *et al* 2004 Overview of LIGO Instrumentation *Proceedings of SPIE* **5500** 11–24 (29 Sept.).

[3] Abbott B P *et al* 2009 LIGO: The Laser Interferometer Gravitational-Wave Observatory *Rep. Prog. Phys.* **72** 076901.

[4] Aston S M *et al* 2012 Update on quadruple suspension design for Advanced LIGO *Class. Quantum Grav.* **29** 235004 (25pp).

[5] Heptonstall A *et al* 2011 Invited Article: CO_2 laser production of fused silica fibers for use in interferometric gravitational wave detector mirror suspensions *Rev. Sci. Instrum.* **82** 011301 1–9.

[6] Cumming A V *et al* 2012 Design and development of the advanced LIGO monolithic fused silica suspension *Class. Quantum Grav.* **29** 035003 (18pp).

[7] *Hamamatsu* S2551 photodiode: http://www.hamamatsu.com/.

[8] Lockerbie N A and Tokmakov K V and Strain K A 2014 A source of illumination for low-noise 'Violin-Mode' shadow sensors, intended for use in interferometric gravitational wave detectors *Meas. Sci. Technol.* **25**,12, 12 p., 125111; http://dx.doi.org/10.1088/0957-0233/25/12/125111.

[9] Lockerbie N A and Tokmakov K V 2014 A 'Violin-Mode' shadow sensor for interferometric gravitational wave detectors *Meas. Sci. Technol.* **25**, 12, 12 p., 125110; http://dx.doi.org/10.1088/0957-0233/25/12/125110.

[10] Dmitriev A *et al* 2010 Controlled damping of high-Q violin modes in fused silica suspension fibers. *Class. Quantum Grav.* **27** 025009 (8pp).

[11] Lockerbie N A and Tokmakov K V 2014 A low-noise transimpedance amplifier for the detection of 'Violin-Mode' resonances in advanced LIGO suspensions *Rev. Sci. Instrum.*, **85**, 11, 8 p., 114705; http://dx.doi.org/10.1063/1.4900955.

[12] Lockerbie N A and Tokmakov K V 2014 Quasi-static displacement calibration system for a 'Violin-Mode' shadow-sensor in Advanced LIGO suspensions *Rev. Sci. Instrum.*, **85**, 10, 12 p., 105003; http://dx.doi.org/10.1063/1.4900955.

[13] Circuit derived from an article by Lukasz Sliwczynskia and Marcin Lipinski, Institute of Electronics, Krakow, Poland, EDN, 1 September,1998, p92.

[14] Lockerbie N A *et al* 2011 First results from the 'Violin-Mode' tests on an advanced LIGO suspension, at MIT. *Class. Quantum Grav.* **28** 245001 (12pp).

[15] Instrument Science White Paper 2012 LIGO-T1200199-v2, p71 https://dcc.ligo.org.